Dynamics of bottlebrush polymers

Karin J. Bichler[1*], *Bruno* Jakobi[1], and *Gerald J.* Schneider[1,2†]

[1]Department of Chemistry, Louisiana State University, Baton Rouge 70803, Louisiana, United States
[2]Department of Physics and Astronomy, Louisiana State University, Baton Rouge 70803, Louisiana, United States

Abstract. Bottlebrushes are an interesting class of polymers which shows intriguing material properties often associated with dynamics. While dynamical phenomena in linear polymers are well understood and existing theories can describe them in a good way, bottlebrush dynamics have only rarely been investigated. Therefore, we performed dielectric spectroscopy and quasi-elastic neutron scattering to study the dynamics of polydimethylsiloxane-based bottlebrush polymers, PDMS-g-PDMS focusing mostly on the segmental dynamics of the side chains. Comparing the relaxation times of the α – relaxation, tracked with dielectric spectroscopy, of bottlebrush polymers with those of their respective linear side chains show a slowing down once the side chains are attached to the backbone. This effect diminishes and finally vanishes with increasing side chain length. The time and length scale, offered by quasi-elastic neutron scattering, fits for the segmental dynamics together with faster processes. The Q-dependence of the segmental relaxation times allows to classify bottlebrush polymers as heterogenous including a non-Gaussian character. For such a dynamical system, the mean square displacement needs to be separated into single processes before an overall mean square displacement can be generated by applying the time temperature superposition principle.

1 Introduction

Graft polymers consist of linear chains chemically attached to a linear backbone. Depending on the grafting density, i.e., the number of side chains per backbone repeating unit, the resulting polymer is either a comb-, or a bottlebrush polymer. At the higher grafting densities of bottlebrushes extraordinary properties like supersoftness, or hyperelasticity emerge.[1] Additionally the entanglement molecular weight shifts to higher values[2] and due to permanent grafting micro or full separation of side chains and backbone is avoided.

Most dynamical studies concentrate on rheology and dielectric spectroscopy.[3-11] A recent dielectric study by Iwawaki *et al.* focuses on bottlebrush polymers having polyisoprene (PI) as backbone and polystyrene (PS) as side chains.[4] A 4-fold increased mean square end-to-end distance, $\langle \vec{R}^2 \rangle$, compared to linear PI with the same number of repeating unites at the bottlebrush backbone was deducted from the dielectric relaxation strength. Viscoelastic spectra on the same PI-g-PS samples are similar to those of linear PI, but with the PI backbone in the bottlebrush being stretched and stiffened.[4] Grigoriadis *et al*. compared bottlebrush polymers with PBiBEM backbone and PBA side chains with the linear counter parts. Hereby, the segmental dynamics of the side chains are slowed-down, while the backbone dynamics are plasticized by the attached side chains.[3] Rheological studies based on grafting density and overall molecular weight were investigated by Haugan *et al.* proposing relationships of the ratio of the diameter of gyration of the side chains, d_{sc}, and the average backbone contour length between grafted chains, L_g, for thin flexible chain behaviour, $\frac{d_{sc}}{L_g} < 1$, and for a behaviour similar to thick semiflexible cylinders, $\frac{d_{sc}}{L_g} > 1$.[9]

Generally, bottlebrush polymers can be achieved via three different synthetic routes, I. Grafting-to, II. Grafting-from, and III. Grafting-through:[10, 12, 13]

While grafting-to (**Fig.1**) is the only method which allows to characterize side chain and backbone separately and independently based on their molecular weight, it is also challenging to achieve high grafting densities due to steric hindrances caused by already grafted side chains.

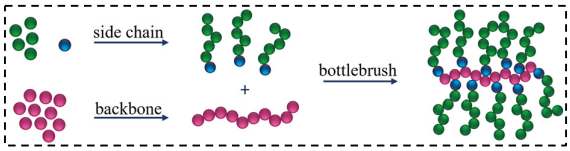

Fig. 1. Illustration of the grafting-to process.

Grafting-from (**Fig. 2**) leads to synthesising the backbone first, with the possibility to determine the molecular weight, and subsequently, the side chains are polymerized directly from the functionalized backbone. This could lead to lower than expected grafting densities and uncertainties in the determination of the molecular

* Corresponding author: kbichler@lsu.edu,
† Corresponding author: gjschneider@lsu.edu

weight and molecular weight distribution of the side chains.

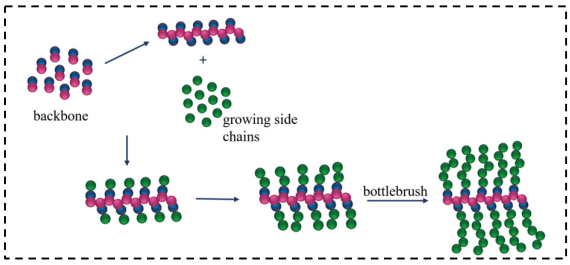

Fig. 2. Illustration of the grafting-from process.

The most promising way is the grafting-through (**Fig. 3**) method. It is based on synthesising macromonomers and enables 100% grafting densities, whereby the molecular weight of the side chains can be determined in advance.

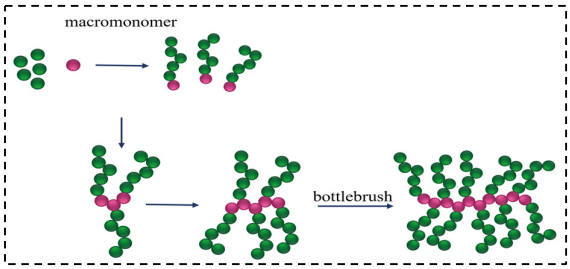

Fig. 3. Illustration of the grafting-through process.

As seen, each method has advantages and disadvantages. Additionally, to that, the choice of synthesis route is restricted by the targeted polymer. In our case, we have used polydimethylsiloxane (PDMS) for side chains and backbone which limits us to the grafting-to method. Using anionic ring opening polymerization in combination with chlorination of the backbone and a mild grafting reaction of silanol terminated side chain precursors results in the PDMS-g-PDMS bottlebrush polymers as shown in **Fig. 4**.[14, 15]

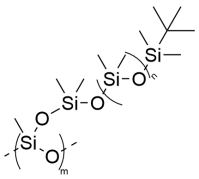

Fig. 4. Chemical structure of PDMS-g-PDMS bottlebrush polymer.[15]

For the structure, by changing the ratio of the degree of polymerization, DP, from backbone and side chains results in a shape transition from elongated objects for $\frac{DP^{side\ chain}}{DP^{backbone}} < 1$, to more spherical ones in case of $\frac{DP^{side\ chain}}{DP^{backbone}} > 1$.[16, 17] This means, by increasing the side chains length, while decreasing the backbone length different shapes are induced.

For our experiments, we have chosen three different combinations of side chain to backbone lengths, while the backbone was roughly constant for all samples. As shown in table 1, Sample 1 has the shortest side chains, resulting in an elongated object.[15] Going to Sample 3 the side chain length increases to be comparable with the length of the backbone. This leads to more spherical objects, confirmed by small-angle neutron scattering (SANS).[15]

Table 1. Number average molecular weight, M_n, of side chains, backbones, and the entire bottlebrush polymer.

Name	$M_n^{side\ chain}$ (g/mol)	$M_n^{backbone}$ (g/mol)	$M_n^{bottlebrush}$ (kg/mol)
Sample 1	298	16500	95
Sample 2	1800	13500	157
Sample 3	11500	13500	1106

2 Dynamics

2.1 Broadband Dielectric Spectroscopy

Dynamical studies have been performed using broadband dielectric spectroscopy (BDS). Hereby, the sample was placed between two gold electrodes with 0.1 mm thick glass spacers for ensuring a constant sample thickness. Depending on the frequency, the fluctuations of the permanent dipole moments are detected, giving relaxation peaks in the imaginary part of the complex permittivity, $\epsilon''(\omega)$ vs. ω. The dynamical information obtained from BDS depends on the orientation of the permanent dipole moments. In case of the parallel component, information about the fluctuations of the chain end-to-end vector, also known as normal mode, are obtained. The component perpendicular to the polymer chain, gives information about the dynamics of the segments, i.e., α – relaxation.[18]

The used polymer, PDMS, has only a perpendicular component, thus the tracked dynamical process is the segmental dynamics. Most of the dipole moments are located within the side chain of the bottlebrush polymers, therefore, the measured signal is dominated by the dynamics of the side chains.

As seen in **Fig. 5**, with increasing temperature, the relaxation peak shifts to higher frequencies.

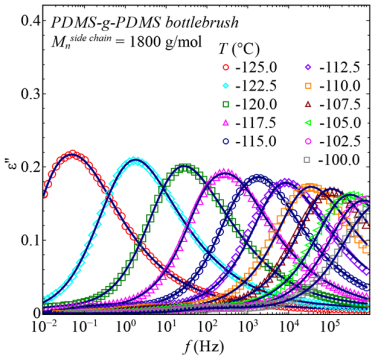

Fig. 5. Imaginary part of the dielectric permittivity, ϵ'', as a function of frequency, f, for Sample 2 for different temperatures as indicated. Solid lines are the best descriptions with Havriliak Negami functions. Data has been previously published in Jakobi *et al*.[15]

Due to the connection of relaxation time and frequency, $\tau \propto 1/f$, it is clearly seen that the relaxation time decreases, thus the relaxation itself speeds up. This experiment has been done for each bottlebrush polymer and for each respective single linear side chain. For a better comparison of the relaxation behaviour, within each set, we compare the temperature dependence of the relaxation times as shown in **Fig. 6**.

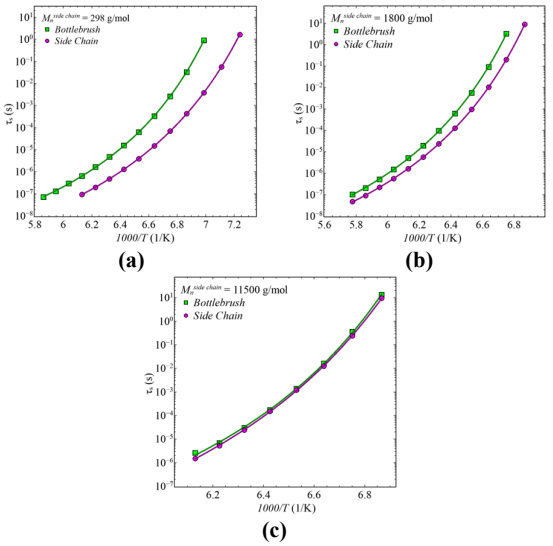

Fig. 6. Segmental relaxation time, τ_s, as a function of $1000/T$ for each bottlebrush polymer in comparison with their respective single linear side chain. **(a)** Sample 1, **(b)** Sample 2, and **(c)** Sample 3. Solid lines are the best description with the VFT equation. Data has been previously published in Jakobi *et al*.[15]

Comparing the shortest single side chains with the bottlebrush (Sample 1), a reduction of the segmental relaxation time, τ_s, of more than one order of magnitude is visible in the investigated temperature range. Increasing the side chain length across the three samples, leads to approaching segmental relaxation times with roughly half a decade difference (Sample 2) and finally to an almost identical relaxation time behaviour of both, single side chain and bottlebrush polymer (Sample 3) over the entire temperature range. This indicates that the inner segments of the side chains are influenced the most by the connection to the backbone leading to the observed slowed down process of the segmental relaxation time. With increasing side chain length, this effect levels off, since with increasing distance a decreasing correlation is expected. Hence, outer segments have the lowest correlation. As Figure 6 c) illustrates this leads to a relaxation time identical to freely moving chains, which implies that the number of segments that have lost correlation to the grafting point dominates.

Additionally, dielectric spectroscopy allows to extract the sample specific glass transition temperature, T_g, using the relationship of $\tau_s(T_g) = 100$ s.[19] Accounting for the different T_g of our samples by scaling the temperature axis to $T - T_g$ reveals differences in relaxation behaviour beyond those associated with different glass transition temperatures (**Fig. 7**).

As seen in **Fig. 7**, sample 2 and sample 3 show almost identical relaxation behaviour over the entire temperature range, while relaxation times of sample 1 indicate some minor differences but only at higher temperatures. Even after eliminating effects associated with T_g, the shortest side chains appear to be faster than the associated bottlebrush polymers. This observation seems to be similar to the strong influence of branching and functional end groups on the glass transition temperature as reported by Khalyavina *et al*.[20]

2.2 Quasi-Elastic Neutron Scattering

Stimulated by the results of dielectric spectroscopy (**Fig. 6**), quasi-elastic neutron scattering (QENS) experiments have been performed to elaborate on the segmental dynamics of bottlebrush polymer more in detail with the advantage of time and length scale information simultaneously. To maximize time coverage, a combination of three different spectrometers – EMU and Pelican at ANSTO, Sydney, Australia, and IRIS at ISIS in Didcot, UK – in the time domain was used, whereby the sample was placed in annular aluminium sample cans with sample thickness of 0.1 mm. QENS is sensitive to the incoherent scattering cross section which is most pronounced for protons. Most of the protons in our samples are located within the side chains, thus the dominating contribution to the scattering signal originates from dynamical processes within the side chains of the bottlebrush polymer. These processes include methyl group rotation at very low temperatures and segmental dynamics, both confirmed by the elastic fixed window scan prior to the quasi-elastic scans.

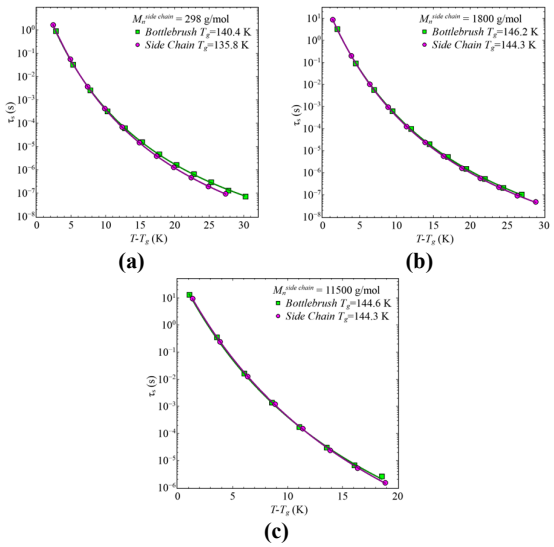

Fig. 7. Segmental relaxation time, τ_s, as a function of $T - T_g$ for each bottlebrush polymer in comparison with their respective single linear side chain. **(a)** Sample 1, **(b)** Sample 2, and **(c)** Sample 3. Solid lines are the best description with the VFT equation.

As typical for localized motion like the methyl group dynamics, a very weak decay with Q-independent

relaxation time is observed for the intermediate scattering function, $S(Q,t)$, as displayed in **Fig. 8**.

With increasing the temperature from $T = 75$ K to $T = 175$ K, a plateau establishes for $t > 0.1$ ns which indicates confined motion for the methyl group dynamics. Hereby, the experimental data were described by

$$S_l(Q,t) = A \cdot DWF \times \left(EISF + (1 - EISF) \cdot \exp\left(-\left(\frac{t}{\tau_l}\right)^{\beta_l}\right)\right) \quad (1)$$

including the Debye-Waller factor, DWF, accounting for fast vibrations and the Elastic Incoherent Structure Factor, $EISF$, describing the confined nature of the localized motion. This allowed to quantify the confinement of the methyl group rotation as the three-fold jump, typical for that relaxation.[14, 21]

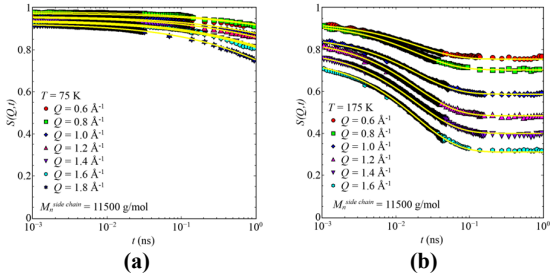

(a) **(b)**

Fig. 8. Intermediate scattering function, $S(Q,t)$, as a function of time, t, for Sample 3 for two selected temperatures, **(a)** $T = 75$ K, and **(b)** $T = 175$ K. Solid lines are the best description with the model function, equation (1). Data has been previously published at Bichler *et al.*[14]

Considering the relaxation times of this localized motion, τ_l, shows an independence on the side chain length additionally to the independence on the momentum transfer as seen in intermediate scattering function, $S(Q,t)$. The temperature dependence of the localized motion shows a well pronounced Arrhenius behaviour, indicative for thermally activated processes. An activation energy, E_A, of ~6 kJ/mol needs to be applied per three-fold jump, a value comparable in order of magnitude with those reported for other methyl group rotations.[14]

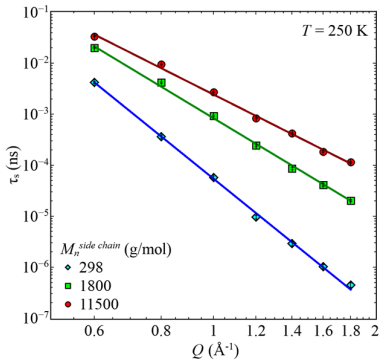

Fig. 9. Segmental relaxation time, τ_s, as a function of momentum transfer, Q, for all three samples at T = 250 K. Solid lines are the descriptions with the power law with exponents, $-s = 7.2$ (blue diamonds, Sample 1), $-s = 5.0$ (green squares, Sample 2), and $-s = 4.2$ (red circles, Sample 3). Data has been previously published at Bichler *et al.*[14]

Increasing the temperature to $T = 250$ K, shifts the segmental relaxation inside the available time range. Hereby, the intermediate scattering function is fully decaying to zero with an Q-dependent relaxation time. After describing the data with

$$S_s(Q,t) = A \cdot DWF \cdot \exp\left(-\left(\frac{t}{\tau_s}\right)^{\beta}\right) \quad (2)$$

the obtained relaxation time, τ_s shows a well pronounced power law dependence on the momentum transfer, changing with side chain length (**Fig. 9**).

With increasing side chain lengths, the relaxation time slows down together with increasing power law dependence on Q, reaching from -7.2 to -4.2, directing to faster dynamics at shorter length scales. This substantial decrease can be better understood by a comparison with the momentum transfer dependence observed for linear chains. Typically, $\tau_s \propto Q^{-4}$, corresponding to a stretching parameter of $\beta_s = 0.5$ is observed, which implies that sufficiently long side chains may approach the values of linear chains. This observation is consistent with the relaxation times for the free and the side chains which become similar for longer side chains.

The power law dependence allows to classify our systems either as homogenous or heterogenous. In case of homogenous behaviour, $\tau_s \propto Q^{-s}$ with $s = 2/\beta_s$ needs to be fulfilled. This would require that we need to be able to describe our power laws depending on the stretching parameters, s vs. β_s, with $s = 2/\beta_s$, which would correspond to the green line in **Fig. 10**.

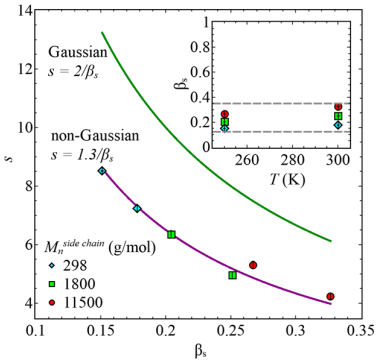

Fig. 10. Power law, s, as a function of stretching parameter, β_s, for all three sample and both temperatures, $T = 250$ K, and $T = 300$ K. Sold green lines corresponds to Gaussian behaviour for a homogenous system. Solid purple line corresponds to $s = 1.3/\beta_s$. Data has been previously published at Bichler *et al.*[14]

However, the obtained data are below the description for homogeneous system and therefore, pointing to a heterogenous system in all three cases. This heterogeneity is induced by two different origins. One is coming from the combination of different dynamical processes for momentum transfers $Q \geq 0.6$ Å^{-1}. The second heterogeneity is based on the intrinsic heterogeneity of the segmental relaxation which is enhanced by the branched nature of the bottlebrush polymer. Grafting side chains to

a backbone broadens the distribution of segmental relaxation times, and thus increases the heterogeneity.

These heterogeneities are considered via the non-Gaussian parameter, $\alpha_2(t)$, which can be incorporated for the mean square displacement.

$$S(Q,t) = A \cdot \exp\left(-\frac{\langle r^2(t)\rangle}{6}Q^2 + \frac{\langle r^2(t)\rangle^2 \alpha_2(t)}{72}Q^4\right) \quad (3)$$

Hereby, $\alpha_2(t) \neq 0$ indicates deviations from a Gaussian distribution of relaxation times, and therefore deviations from homogeneous dynamics.

As seen in **Fig. 11** with increasing temperature, $\alpha_2(t)$ decreases which is attributed to a reduced heterogeneity at higher temperatures. In all cases, $\alpha_2(t)$ approximates zero for long times indicating the complete relaxation of all processes in the available time frame.

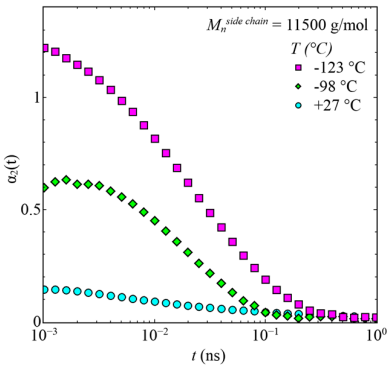

Fig. 11. Non-Gaussian parameter, $\alpha_2(t)$, as a function of time, t, for Sample 3 at selected temperatures. Data has been previously published at Bichler *et al.*[22]

Using equation (3) not only gives access to the non-Gaussian parameter, but we also obtain the mean square displacement, $\langle r^2(t)\rangle$, for each temperature and each sample, as shown in **Fig. 12** for Sample 3.

Clearly two distinct regions emerge, one at higher temperatures, describing the segmental dynamics and one at lower temperatures accounting for the methyl group dynamics. The plateau at long times indicates the confined nature of the methyl group rotations.

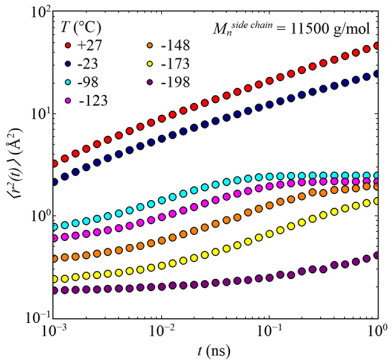

Fig. 12. Mean square displacement, $\langle r^2(t)t\rangle$, as a function of time, t, for Sample 3 at different temperatures as indicated. Data has been previously published at Bichler *et al.*[22]

Due to the similarity of each mean square displacement in each temperature region, time temperature superposition (TTS) principle has been applied to increase the available time range. However, simply shifting them together violates TTS due to discrepancies at short and long times for both regions.[22] This is caused by the mixture of different process of different length scales, causing the heterogeneity. Removing those faster contributions and reducing the mean square displacement to one single process, i.e., either pure methyl group or pure segmental relaxation, results in overlapping data over the whole time range (**Fig. 13**).

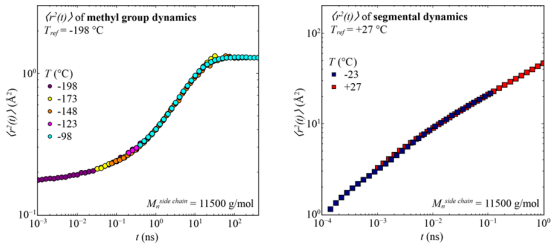

(a) **(b)**

Fig. 13. Mean square displacement, $\langle r^2(t)\rangle$, as a function of time, t, for Sample 3. **(a)** pure methyl group dynamics. **(b)** pure segmental dynamics. Data has been previously published at Bichler *et al.*[22]

This leads to the conclusion, that TTS is fulfilled as long as only one process occurs in the observed time frame, without any contribution from others. Further, both single mean square displacements have been combined at one reference temperature by shifting them accordingly to the shift parameter, obtained either from dielectric spectroscopy or from the quasi-elastic scans. These two shifted $\langle r^2(t)\rangle$ have been added pointwise resulting in the combined mean square displacement containing methyl group and segmental dynamics.

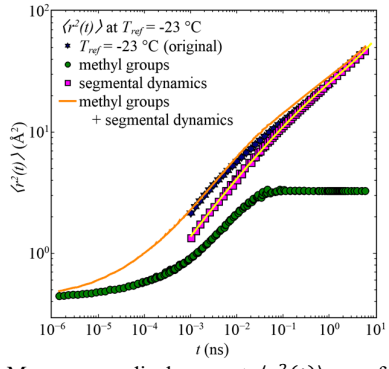

Fig. 14. Mean square displacement, $\langle r^2(t)\rangle$, as a function of time, t, for Sample 3. Data has been previously published at Bichler *et al.*[22]

As seen by the comparison of the generated mean square displacement, (**Fig. 14**, orange solid line), with the original $\langle r^2(t)\rangle$ obtained from $S(Q,t)$ at that specific reference temperature (**Fig. 14**, blue stars) the used approach can recover the original data well over an enlarged temperature range even across the glass

transition temperature where usually the TTS is known to break down (**Fig. 14**).

Finally, the fast vibrations have been added for all three samples resulting in three different power law regions over the achieved time range as seen in **Fig. 15**. At very short times, accounting for vibrations and methyl group dynamics, the power law of $t^{0.1}$ does not change while changing the side chains length. Continuing to intermediate times, where a combination of methyl group and segmental dynamics occurs, the power law changes from $t^{0.35}$ to $t^{0.4}$. Since the relaxation of methyl groups is independent on the side chains length, this power law change could be due to the onset of segmental dynamics. At the long times the power law changes from $t^{0.2}$ to $t^{0.3}$. In this time range, the methyl group dynamics goes into a plateau and gives a constant contribution. Therefore, the change in power is entirely from the segmental dynamics. This change let's assume that with increasing side chain length, i.e., increasing distance from the backbone, the segmental dynamics has less confinement and eventually reaches the behaviour of a linear polymer chain ($t^{0.5}$).

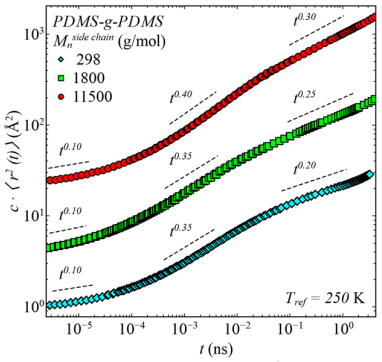

Fig. 15. Mean square displacement, $\langle r^2(t) \rangle$, as a function of time, t, for all three samples. Data has been previously published at Bichler *et al.*[22]

Summary and Conclusions

Dynamical studies on bottlebrush polymers using dielectric spectroscopy and quasi-elastic neutron scattering revealed more detailed insights to this polymer architecture. Since the majority of the permanent dipole moments, for dielectric spectroscopy, as well as most of the protons, for quasi-elastic neutron scattering, are located within the side chains, the information obtaining from the experiments is for the side chain dynamics. In our study, we focused on dynamical changes inherent with increasing side chain lengths of the bottlebrush polymers. This further induced the shape transition from elongated objects into more spherical ones. Based on dielectric spectroscopy, a slowed down process is observable by comparing side chains of the bottlebrush polymer with their respective single linear chains. This effect vanishes for sufficiently long side chains. Within the time and temperature range of quasi-elastic neutron scattering experiments, the methyl group and segmental dynamics of the side chains were tracked. Hereby, the methyl group rotations are independent on the length scale and the side chain length but confined on a characteristic three-fold jump. In contrast the segmental dynamics depends on the side chain length and shows a particular Q-dependence. This power law dependence allows to categorize the bottlebrush polymers as heterogenous systems with the non-Gaussian parameter incorporated into the mean square displacement analysis. Hereby, two distinct regions in $\langle r^2(t) \rangle$ representing the methyl group and segmental dynamics are obtained. Reducing the mean square displacement to one single dynamical process by separating faster processes opens the way to combine several processes by applying time temperature superposition principle. This is valid over an extended temperature range and even across the glass transition temperature where the TTS is usually known to break down.

We gratefully acknowledge funding by the U.S. Department of Energy (DoE) under grant no. DE-SC0019050.

References

1. L.-H. Cai, T. E. Kodger, R. E. Guerra, A. F. Pegoraro, M. Rubinstein, D. A. Weitz, Adv. Mater., **27**, 5132 (2015)

2. C. Gerstl, G. J. Schneider, A. Fuxman, M. Zamponi, B. Frick, T. Seydel, M. Koza, A. C. Genix, J. Allgaier, D. Richter, J. Colmenero, A. Arbe, Macromolecules, **45**, 4394 (2012)

3. C. Grigoriadis, A. Nese, K. Matyjaszewski, T. Pakula, H.-J. Butt, G. Floudas, Macromol. Chem. Phys., **213**, 1311 (2012)

4. H. Iwawaki, O. Urakawa, T. Inoue, Y. Nakamura, Y. Matsumiya, H. Watanabe, Macromolecules, **53**, 7096 (2020)

5. H. Liang, B. J. Morgan, G. Xie, M. R. Martinez, E. B. Zhulina, K. Matyjaszewski, S. S. Sheiko, A. V. Dobrynin, Macromolecules, **51**, 10028 (2018)

6. M. Hu, Y. Xia, G. B. McKenna, J. A. Kornfield, R. H. Grubbs, Macromolecules, **44**, 6935 (2011)

7. S. J. Dalsin, M. A. Hillmyer, F. S. Bates, ACS Macro Letters, **3**, 423 (2014)

8. S. J. Dalsin, M. A. Hillmyer, F. S. Bates, Macromolecules, **48**, 4680 (2015)

9. I. N. Haugan, M. J. Maher, A. B. Chang, T.-P. Lin, R. H. Grubbs, M. A. Hillmyer, F. S. Bates, ACS Macro Letters, **7**, 525 (2018)

10. M. Abbasi, L. Faust, M. Wilhelm, Adv. Mater., **31**, 1806484 (2019)

11. S. Alexandris, K. Peponaki, P. Petropoulou, G. Sakellariou, D. Vlassopoulos, Macromolecules, **53**, 3923 (2020)

12. R. Verduzco, X. Li, S. L. Pesek, G. E. Stein, Chem. Soc. Rev., **44**, 2405 (2015)

13. T. Pan, S. Dutta, Y. Kamble, B. B. Patel, M. A. Wade, S. A. Rogers, Y. Diao, D. Guironnet, C. E. Sing, Chem. Mater., **34**, 1990 (2022)

14. K. J. Bichler, B. Jakobi, V. G. Sakai, A. Klapproth, R. A. Mole, G. J. Schneider, Macromolecules, **53**, 9553 (2020)

15. B. Jakobi, K. J. Bichler, A. Sokolova, G. J. Schneider, Macromolecules, **53**, 8450 (2020)

16. K. J. Bichler, B. Jakobi, S. O. Huber, E. P. Gilbert, G. J. Schneider, Macromolecules, **53**, 78 (2020)

17. S. L. Pesek, X. Li, B. Hammouda, K. Hong, R. Verduzco, Macromolecules, **46**, 6998 (2013)

18. F. Kremer, A. Schönhals, *Broadband Dielectric Spectroscopy*. Springer Berlin Heidelberg: 2012.

19. J. Hintermeyer, A. Herrmann, R. Kahlau, C. Goiceanu, E. A. Rössler, Macromolecules, **41**, 9335 (2008)

20. A. Khalyavina, L. Häußler, A. Lederer, Polymer, **53**, 1049 (2012)

21. R. Zorn, B. Frick, L. Fetters, JCP, **116**, 845 (2002)

22. K. J. Bichler, B. Jakobi, V. G. Sakai, A. Klapproth, R. A. Mole, G. J. Schneider, Nano Lett., **21**, 4494 (2021)